and solvent in ion permeation. *J. Gen. Physiol.* (in the press).
16. Åqvist, J. & Luzhkov, V. Ion permeation mechanism of the potassium channel. *Nature* **404,** 881–884 (2000).
17. Luzhkov, V. B. & Åqvist, J. K^+/Na^+ selectivity of the KcsA potassium channel from microscopic free energy perturbation calculations. *Biochim. Biophys. Acta* **1548,** 194–202 (2001).
18. Allen, T. W., Bliznyuk, A., Rendell, A. P., Kyuucak, S. & Chung, S. H. The potassium channel: Structure, selectivity and diffusion. *J. Chem. Phys.* **112,** 8191–8204 (2000).
19. Bernèche, S. & Roux, B. Energetics of ion conduction through the K^+ channel. *Nature* **414,** 73–77 (2001).
20. Bernèche, S. & Roux, B. A microscopic view of ion conduction through the K^+ channel. *Proc. Natl Acad. Sci. USA* **100,** 8644–8648 (2003).
21. Shrivastava, I. H., Tieleman, D. P., Biggin, P. C. & Sansom, M. S. P. K^+ versus Na^+ ions in a K channel selectivity filter: A simulation study. *Biophys. J.* **83,** 633–645 (2002).
22. Guidoni, L., Torre, V. & Carloni, P. Potassium and sodium binding to the outer mouth of the K^+ channe. *Biochemistry* **38,** 8599–8604 (1999).
23. Loboda, A., Melishchuk, A. & Armstrong, C. Dilated and defunct K channels in the absence of K^+. *Biophys. J.* **80,** 2704–2714 (2001).
24. Zhou, Y. F. & MacKinnon, R. The occupancy of ions in the K^+ selectivity filter: Charge balance and coupling of ion binding to a protein conformational change underlie high conduction rates. *J. Mol. Biol.* **333,** 965–975 (2003).
25. Yamashita, M. M., Wesson, L., Eisenman, G. & Eisenberg, D. Where metal ions bind in proteins. *Proc. Natl Acad. Sci. USA* **87,** 5648–5652 (1990).
26. Åqvist, J., Alvarez, O. & Eisenman, G. Ion-selective properties of a small ionophore in methanol studied by free energy perturbation simulations. *J. Phys. Chem.* **96,** 10019–10025 (1992).
27. Marrone, T. J. & Merz, K. M. Jr. Molecular recognition of K^+ and Na^+ by valinomycin in methanol. *J. Am. Chem. Soc.* **117,** 779–791 (1995).
28. MacKerell, A. D. J. *et al.* All-atom empirical potential for molecular modeling and dynamics studies of proteins. *J. Phys. Chem. B* **102,** 3586–3616 (1998).
29. Weeks, J. D., Chandler, D. & Andersen, H. C. Role of repulsive forces in determining the equilibrium structure of simple liquids. *J. Chem. Phys.* **54,** 5237–5247 (1971).
30. Lu, T. *et al.* Probing ion permeation and gating in a K^+ channel with backbone mutations in the selectivity filter. *Nature Neurosci.* **4,** 239–246 (2001).
31. Heinemann, S. H., Terlau, H., Stuhmer, W., Imoto, K. & Numa, S. Calcium channel characteristics conferred on the sodium channel by single mutations. *Nature* **356,** 441–443 (1992).
32. Brooks, B. R. *et al.* CHARMM: a program for macromolecular energy minimization and dynamics calculations. *J. Comput. Chem.* **4,** 187–217 (1983).

Supplementary Information accompanies the paper on **www.nature.com/nature**.

Acknowledgements Discussions with G. Eisenman, J. Åqvist, O. Andersen, C. Miller and D. Doyle are gratefully acknowledged. This work was funded by the NIH and by the American Epilepsy Society and UCB Pharma Inc. to S.Yu.N. This work was supported by the National Center for Supercomputing Applications (NCSA) at the University of Illinois, Urbana-Champaign, the Pittsburgh Supercomputing Center (PSC), and the Scientific Computing and Visualization (SCV) group at Boston University.

Competing interests statement The authors declare that they have no competing financial interests.

Correspondence and requests for materials should be addressed to B.R. (benoit.roux@med.cornell.edu).

Low marine sulphate and protracted oxygenation of the Proterozoic biosphere

Linda C. Kah[1], Timothy W. Lyons[2] & Tracy D. Frank[3]

[1]*Department of Earth and Planetary Sciences, University of Tennessee, Knoxville, Tennessee 37996, USA*
[2]*Department of Geological Sciences, University of Missouri, Columbia, Missouri 65211, USA*
[3]*Department of Geosciences, University of Nebraska, Lincoln, Nebraska 68588, USA*

Progressive oxygenation of the Earth's early biosphere is thought to have resulted in increased sulphide oxidation during continental weathering, leading to a corresponding increase in marine sulphate concentration[1]. Accurate reconstruction of marine sulphate reservoir size is therefore important for interpreting the oxygenation history of early Earth environments. Few data, however, specifically constrain how sulphate concentrations may have changed during the Proterozoic era (2.5–0.54 Gyr ago). Prior to 2.2 Gyr ago, when oxygen began to accumulate in the Earth's atmosphere[2,3], sulphate concentrations are inferred to have been <1 mM and possibly <200 μM, on the basis of limited isotopic variability preserved in sedimentary sulphides[4] and experimental data showing suppressed isotopic fractionation at extremely low sulphate concentrations[1,5]. By 0.8 Gyr ago, oxygen and thus sulphate levels may have risen significantly[6,7]. Here we report large stratigraphic variations in the sulphur isotope composition of marine carbonate-associated sulphate, and use a rate-dependent model for sulphur isotope change that allows us to track changes in marine sulphate concentrations throughout the Proterozoic. Our calculations indicate sulphate levels between 1.5 and 4.5 mM, or 5–15 per cent of modern values, for more than 1 Gyr after initial oxygenation of the Earth's biosphere. Persistence of low oceanic sulphate demonstrates the protracted nature of Earth's oxygenation. It links biospheric evolution to temporal patterns in the depositional behaviour of marine iron- and sulphur-bearing minerals[4], biological cycling of redox-sensitive elements[6] and availability of trace metals essential to eukaryotic development[8].

To understand Proterozoic biospheric oxygenation better, we have modified an existing model for C isotope variability[9] to estimate marine sulphate reservoir size using rates of S isotope variation. These rates are recorded stratigraphically as variation in the S isotope composition of evaporitic gypsum and carbonate-associated sulphate (CAS). Because CAS is routinely trapped in marine carbonates[10] and, in organic-poor sediments, is isotopically buffered against appreciable diagenetic overprints[11], it can record the $\delta^{34}S$ signal of marine sea water even when gypsum is lacking. Furthermore, CAS is a more direct proxy for marine sea water than sedimentary pyrite, the isotopic composition of which is complicated by local reservoir effects and varying fractionations during bacterial sulphate reduction (BSR)[12].

In our model, the isotopic composition of marine sulphate changes in response to imbalances in isotopic fluxes into and out of a non-steady state system (see Methods). In the modern ocean, sulphate concentrations of 28.4 mM effectively buffer the isotopic system from changing at rates exceeding 0.5‰ per Myr, despite large fractionations associated with the modern bacterial sulphur cycle (Fig. 1). Long-term variation in the isotopic composition of

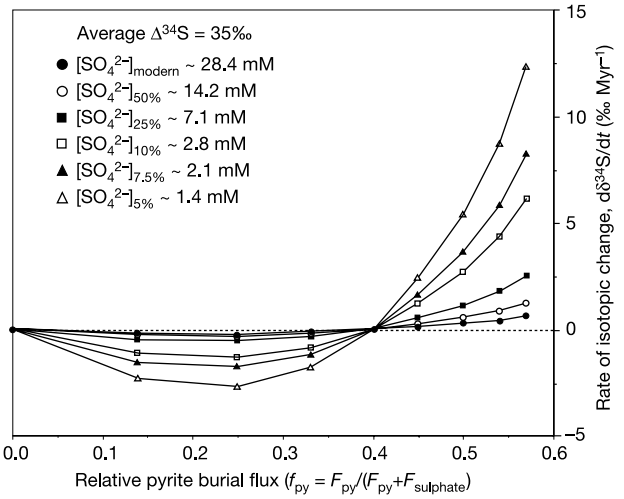

Figure 1 Sensitivity of the marine sulphate system to reservoir size. At average fractionations observed within the modern bacterial sulphur cycle ($\Delta S = 35‰$), modern reservoir sizes effectively buffer the marine system from the large S isotope shifts that characterize Proterozoic stratigraphic sections, even at moderate to high degrees of pyrite burial ($f_{py} = 0.2–0.6$).

marine sulphate from the late Palaeozoic to recent[11,13–15] can then be explained by ±40% variation in weathering (and/or volcanogenic) fluxes and pyrite burial. Increased pyrite burial drives isotopic compositions to higher (more ^{34}S-enriched) δ^{34}S values, and increased weathering results in lower δ^{34}S. When the sulphate reservoir is small, however, flux imbalances can drive much more rapid isotopic variation, such as that observed in Proterozoic successions[16–21].

Samples for CAS analysis were collected from measured stratigraphic sections of the 1.3-Gyr-old Dismal Lakes Group and 1.2-Gyr-old Society Cliffs Formation, Arctic Canada, and extracted via standard methods of acid dissolution and precipitation of CAS as barium sulphate[11,16]. Both units reveal large, systematic shifts in δ^{34}S of up to 12‰ over 300 m in the Society Cliffs and up to 15‰ over 200 m in the Dismal Lakes Group (Fig. 2, and Supplementary Information). Similar patterns of rapid isotopic change are unknown from late Palaeozoic and younger successions but are recorded in both sulphate and sulphide isotopic data from numerous other Proterozoic successions[16–20], suggesting that rapid S isotope change is a common, if not universal, feature of Proterozoic oceans. Furthermore, in the Society Cliffs Formation, CAS data show isotopic trends that mimic (with ~3–5‰ offset) that of interbedded gypsum, the marine origin of which is constrained by Sr isotope and trace element data[21]. Although the cause is unknown, the isotopic offset is small compared to the magnitude of observed shifts, and the consistency of isotopic trends in gypsum and CAS offers unprecedented corroboration that CAS accurately records changes in marine S isotope composition.

Pb–Pb isotope analysis of a stratigraphic suite of carbonate samples provide an age of 1,204 ± 22 Myr for the Society Cliffs and overlying Victor Bay and Athole Point formations (1,750 m total thickness)[21]. If this range, from 1,226 to 1,182 Myr ago, represents the maximum duration of stratal deposition, we can estimate the minimum accumulation rate of the Society Cliffs Formation to be approximately 40 m Myr^{-1}. Similarly, the 1,200-m-thick Dismal Lakes Group is constrained by a combination of radiometric and chemostratigraphic data to have been deposited between 1,300 and 1,270 Myr ago[22], again indicating a minimum accumulation rate of 40 m Myr^{-1}. Despite uncertainty in determining deposition rates for Proterozoic successions, calculated accumulation rates of 40 m Myr^{-1} are similar to minimum accumulation rates (30–80 m Myr^{-1}) observed for Palaeozoic carbonate platforms[23]. A conservative estimate of 30–50 m Myr^{-1} thus provides a reasonable estimate for minimum accumulation rates of shallow marine carbonate successions, even when appropriate time constraints are lacking, and is applied to all model data.

Accumulation rates of 30–50 m Myr^{-1} provide minimum rates of S isotope change of 1.4–2.0‰ Myr^{-1} and 2.6–3.8‰ Myr^{-1} for the Society Cliffs Formation and Dismal Lakes Group, respectively. In terms of our model, these values yield sulphate concentrations of 2.7–4.5 mM for the Society Cliffs Formation and 1.5–2.4 mM for the Dismal Lakes Group, with higher deposition rates resulting in lower sulphate concentrations. Sulphate concentrations of 1.5–4.5 mM, or ~5–15% of modern concentrations, are therefore considered to represent maximum marine sulphate concentrations for the Mesoproterozoic, and are consistent with hypotheses that low-oxygen conditions persisted at least into the Mesoproterozoic[4,8,24].

More importantly, our model provides a mechanism for exploring the long-term dynamics of biospheric oxygenation (Fig. 3, Table 1). CAS data from pericratonal, shallow-water carbonates of the 1.7-Gyr-old McNamara Group, Australia, show little systematic pattern of isotopic change, although data reveal several stratigraphic shifts of up to 10‰ over intervals of 50 m (ref. 19, and Supplemetary Information). These shifts suggest maximum marine sulphate concentrations between 0.5 and 0.9 mM. Because S isotope compositions would have been extraordinarily sensitive to even minor variation in fluxes at these low concentrations, data scatter probably represents local overprinting of global isotopic signals. Despite limitations of these data, our model results are consistent with sulphate concentrations of 0.5–2.0 mM estimated from Fe-S-P flux-based models constructed to explain the persistence of ^{34}S-enriched sulphides at this time[25]. Combined, CAS and Fe-S-P models suggest that increased biospheric oxygen at 2.2 Gyr ago need not have raised oceanic sulphate concentrations appreciably beyond levels estimated for much of the Archaean.

CAS data from the 1.45-Gyr-old Helena Formation, Belt Supergroup, Montana, show stratigraphic changes in S isotope compo-

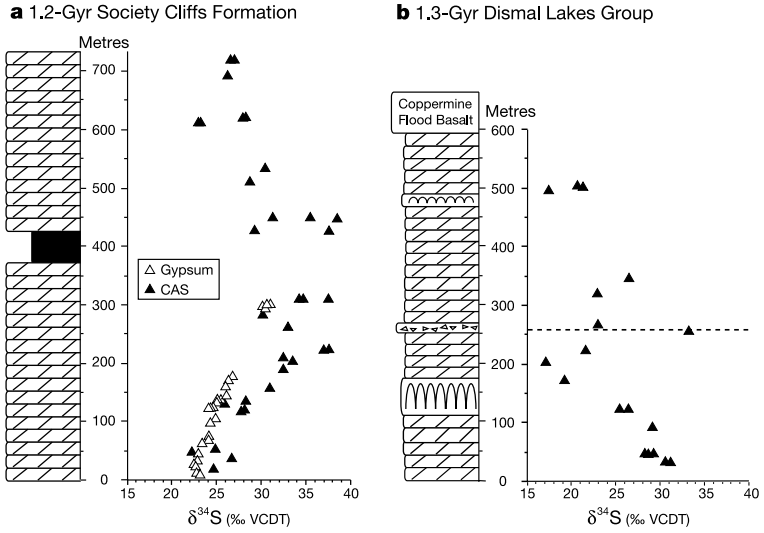

Figure 2 Isotopic composition of CAS from Mesoproterozoic strata. **a**, CAS data from the 1.2-Gyr-old Society Cliffs Formation are similar to S-isotope data from penecontemporaneous gypsum[21] and show correspondingly large stratigraphic shifts in S-isotope composition. **b**, CAS data from the 1.3-Gyr-old Dismal Lakes Group reveals similarly large isotopic shifts, with strong discontinuity apparent only at a major subaerial exposure surface (dotted line). All S isotope compositions are expressed in standard delta notation as per mil (‰) deviations from VCDT, with analytical error of <0.01‰, calculated from replicate analyses of laboratory standards. See Supplementary Information for tabulated data.

sition of up to 15‰ over 200 m (ref. 19). Similar trends are preserved by sulphides in the 1.47-Gyr-old Prichard and Newland formations, Belt Supergroup[12,17], as well as CAS from the 1.3-Gyr-old Dismal Lakes Group, supporting an increase in marine sulphate concentration to approximately 1.5–2.4 mM by this time. Although the paucity of data inhibits detailed reconstruction of marine sulphate concentrations during the Proterozoic, it is clear that sulphate concentrations remained significantly low for at least 900 Myr after initial oxygenation of the Earth's biosphere. By contrast, CAS data from the 1.2-Gyr-old Society Cliffs Formation show stratigraphic changes in S isotope composition that yield estimates of 2.7–4.5 mM sulphate, nearly double that estimated for 1.3-Gyr strata.

In the Neoproterozoic, observed fractionation between coeval sulphate and sulphide increased to ~35‰ (ref. 6), which would have led to increased rates of S isotope change. However, sparse CAS data from the (probably) early Neoproterozoic Vazante Formation, Brazil[20], suggest rates of isotopic change as low as 0.75‰ Myr^{-1}—much lower than those observed in the Mesoproterozoic—suggesting that marine sulphate concentrations may have risen to 6–10 mM, or 20–35% of modern values, by this time. Similarly low rates of isotopic change recorded in interglacial carbonates of the ~740-Myr-old Otavi Group, Namibia (Ombaatjie Formation)[16] suggest sulphate concentrations near 7 mM, or 25% of modern values, may have persisted through much of the Neoproterozoic. In sharp contrast to preglacial and interglacial successions, large and rapid shifts in CAS composition in post-glacial cap carbonates (Rasthof and Maieberg formations) of the Otavi Group[16] suggest marine sulphate concentrations of <1.3 mM and support hypotheses of near complete reduction of the oceanic sulphate reservoir during Neoproterozoic glacial episodes[16]. Together, these data suggest that marine sulphate concentrations probably remained low, <35% of modern values, for nearly the entire Proterozoic. A significant rise in biospheric oxygen, and thus oceanic sulphate, may not have occurred until the latest Neoproterozoic (0.54 Gyr), just before the Cambrian explosion, when sulphate levels may have reached 20.5 mM, or 75% of present-day levels[26].

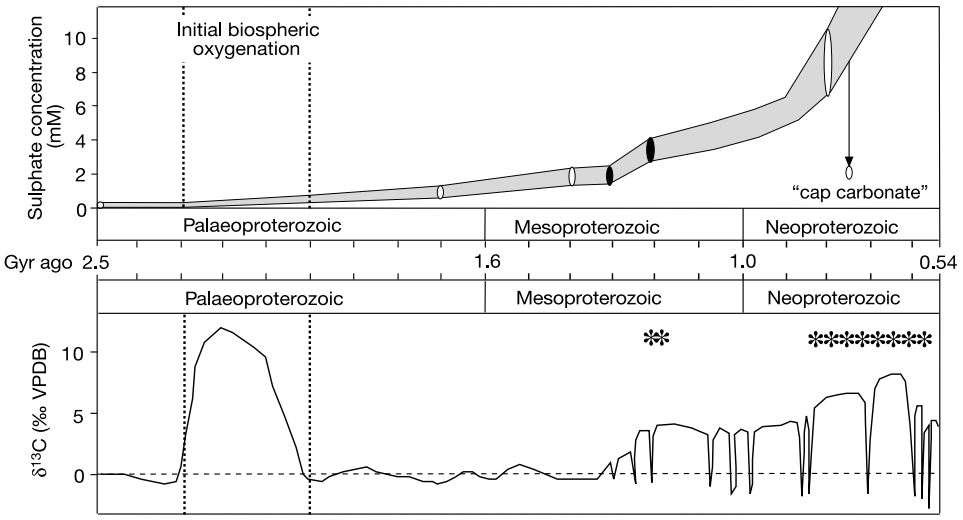

Figure 3 Proterozoic marine sulphate concentrations. Filled ovals mark data from this study; open ovals mark data referred to in the text[4,16,19,20]. Marine sulphate concentrations probably remained below 2 mM until about 1.3 Gyr ago, rose to ~4.5 mM by 1.2 Gyr ago, and possibly as high as 7–10 mM by the mid-Neoproterozoic, although near-complete reduction of oceanic sulphate may have occurred during Neoproterozoic glacial intervals (arrow)[16]. Increased sulphate concentrations coincide with changes in marine $\delta^{13}C$ associated with biospheric oxygenation and are marked by the appearance of bedded gypsum (asterisks) in the late Mesoproterozoic and more frequent gypsum deposition in the Neoproterozoic.

Table 1 **Marine sulphate concentrations for Mesoproterozoic and Neoproterozoic strata**

	Deposition rate, estimated ($m\,Myr^{-1}$)	Observed $d\delta S/dt$ ($‰\,Myr^{-1}$)	Inferred $d\delta S_{max}/dt$ ($‰\,Myr^{-1}$)	Max. $[SO_4^{2-}]$ $\Delta S = 25$ (mM)	Max. $[SO_4^{2-}]$ $\Delta S = 35$ (mM)
~1.7-Gyr McNamara Fm.[19]	30	6.0	60	0.9	*
	50	10.0	100	0.5	
~1.45-Gyr Helena Fm.[19]	30	2.3	26	2.4	*
	50	3.8	38	1.5	
~1.3-Gyr Dismal Lakes Grp	30	2.3	26	2.4	*
	50	3.8	38	1.5	
~1.2-Gyr Society Cliffs Fm.	30	1.4	14	4.5	*
	50	2.0	20	2.7	
~750-Myr Vazante Fm.[20]	30	0.8	7.5	*	10.1
	50	1.3	12.5		6.1
~740-Myr Otavi Grp[16]	30	1.1*	10.5	*	7.2
	50	1.8*	17.5		2.8
~740 Myr Otavi Grp[16]	30	6.0†	60	*	1.3
	50	10.0†	100		0.8

Marine sulphate concentrations are calculated from CAS data.
*Reported values are estimates of S isotope change recorded in the Ombaatjie Formation, which was deposited during a Neoproterozoic interglacial period.
†Reported values are estimates of S isotope change in 'cap carbonate' strata, which directly overlie glacial diamictites and are believed to record Neoproterozoic glacial conditions. See text for details.

Increases in oceanic sulphate in both the mid-Mesoproterozoic and Neoproterozoic are temporally consistent with abrupt changes in the C isotope record (Fig. 3) and inferred increases in biospheric oxygenation[3,21,27], and are reflected in the geologic history of marine gypsum deposition. In the presence of available Ca, late Mesoproterozoic sulphate concentrations of 2.7–4.5 mM would require >95% reduction in water volume in order to reach gypsum saturation. If, at this time, Ca availability was limited by excess precipitation of calcium carbonate resulting from elevated carbonate saturation[28], an even greater degree of evaporation would be required to reach gypsum saturation. In either case, estimated sulphate concentrations are consistent with rare bedded gypsum in the late Mesoproterozoic and apparent deposition of halite before gypsum[21]. In comparison, lower sulphate concentrations before 1.3 Gyr ago would probably result in only isolated occurrences of gypsum, and more frequent gypsum deposition would not be expected to occur until the Neoproterozoic, when sulphate concentrations may have reached at least 25% of modern values.

Calculations presented here suggest that marine sulphate concentrations, and thus biospheric oxygen levels, though increasing, remained low through at least the Mesoproterozoic, and probably well into the Neoproterozoic. This interpretation is consistent with the possibility of long-term, anoxic deep-ocean conditions during the Proterozoic[4,8,24]. The data, however, do not specifically indicate the presence of sulphide in the water column. Sulphate concentrations as low as 1–2 mM may have persisted for nearly 1,000 Myr after initial biospheric oxygenation. Increasing sulphate concentrations within an oxygen-deficient deep ocean would have supported the development of widespread sulphidic (euxinic) bottom waters[4]. The ubiquity of sulphidic waters in turn may have affected the ecological and evolutionary development of eukaryotes via limitation of redox-sensitive bioessential nutrients[8]. In this light, further increases in atmospheric and thus oceanic oxygenation, as delineated by our estimates for seawater sulphate, are consistent with independent evidence for eukaryotic diversification in the late Mesoproterozoic and Neoproterozoic. Our model for rates of isotopic change in the marine sulphate reservoir thus provides a window into early Earth oxygenation, and establishes a framework for continued examination of Proterozoic biospheric evolution. □

Methods

Sulphate reservoir size is estimated from the relationship $[d\delta_{sulphate}/dt] = [F_w(\delta_w - \delta_{sulphate}) - F_{py}\Delta S]/M_o$, where F_w is the total input flux of sulphur to the ocean–atmosphere system from weathering, δ represents the isotopic composition of fluxes associated with weathering and sulphate deposition ($\delta^{34}S$ in ‰ $= [(^{34}S/^{32}S)_{sample}/(^{34}S/^{32}S)_{standard} - 1] \times 1{,}000$ relative to the Cañon Diable Troilite standard), M_o is the mass of sulphur in the oceans as sulphate, and ΔS is the observed fractionation between oxidized and reduced sulphur reservoirs ($\Delta S = \delta_{sulphate} - \delta_{sulphide}$) expressed as a negative number. In the model, F_{py} is allowed to vary, and $\delta_{sulphate}$ varies according to the equation $\delta_{sulphate} = \delta_w - (\Delta S f_{py})$, where $f_{py} = F_{py}/(F_{sulphate} + F_{py})$, representing the relative rate of pyrite burial. Estimates for modern fluxes and their isotopic compositions are as follows: $M_o = 1.3 \times 10^{21}$ g, $F_w = 1.0 \times 10^{14}$ g yr^{-1}, $\delta_w = 6$‰, $F_{sulphate} = 6 \times 10^{13}$ g yr^{-1}, $F_{py} = 4 \times 10^{13}$ g yr^{-1}, $\Delta S = 35$‰ (refs 29, 30).

Following from $[d\delta_{sulphate}/dt] = [F_w(\delta_w - \delta_{sulphate}) - F_{py}\Delta S]/M_o$, maximum rates of isotopic change are reached when S input to the oceans approaches zero ($F_w' = 0$) and the standing marine sulphate reservoir is removed as pyrite ($F_{py}' = F_w$), giving $[d\delta_{max}/dt] = [F_w\Delta S]/M_o$ or $d\delta_{max}/dt = \Delta S/T_R$ where ΔS is the average maximum fractionation during BSR and T_R is the residence time for sulphate in the oceans [$T_R = M_o/F_w$]. Sulphate residence time is approximately 13 Myr in the modern ocean[29].

In the present study, sulphate reservoir size (in grams S as sulphate) is calculated as $M_o = [F_w\Delta S]/[d\delta_{max}/dt]$. S isotope trends for late Palaeozoic and younger strata[11,13,14] indicate that natural variation in the rates and isotopic composition of weathering and pyrite burial fluxes result in rates of isotopic change ($d\delta_{sulphate}/dt$) that reflect only 3–14% of maximum possible rates of isotopic change ($d\delta_{max}/dt$). Observed variation in Proterozoic isotopic records is therefore estimated to represent 10% of maximum values. See Supplementary Information for graphical representation of model sensitivities.

In this model, M_o is most sensitive to changes in ΔS, wherein a 10% change in ΔS (~5‰) results in a 0.7 mM change in M_o. In laboratory experiments, single-step, dissimilatory sulphate reduction can achieve fractionations up to 40–45‰, and disproportionation in the oxidative part of the bacterial sulphur cycle can produce fractionations >45‰ (refs 1, 6). These high values, however, are rare in many natural systems[5]. Heavier values typically preserved in the geologic record reflect the integration of bacterial fractionation during progressive depletion of sulphate in sedimentary pore waters during BSR[5]. In our calculations, we have allowed the average maximum fractionation during BSR (ΔS) to vary with time as indicated by empirical data recorded in Proterozoic strata. Prior to ~850 Myr ago, observed maximum values for ΔS rarely exceeded an average of 25–30‰ (ref. 6); after ~850 Myr ago, when biospheric oxygen levels may have facilitated enhanced fractionations, in part through bacterial disproportionation pathways, observed maximum values for ΔS increase to an average of ~35‰ (refs 6, 29). Although ΔS values <25‰ are not uncommon in the Proterozoic[6], the presence of high ΔS values (25‰ and 35‰, respectively) suggests that Meso- to Neoproterozoic open marine systems may have supported only limited renewal of sulphate to the site of BSR[12], resulting in heavy values representative of suppressed net bacterial fractionation.

Calculations of M_o are least sensitive to changes in F_w. In our model, a 10% decrease in F_w results in a 0.3 mM reduction in M_o. In the Proterozoic, lower atmospheric oxygen would have resulted in a decrease in the oxidative weathering of sulphate to the oceans. Yet because of uncertainties regarding the magnitude of Proterozoic weathering, we have used modern weathering fluxes to ensure that our calculations reflect maximum values for M_o.

In contrast to ΔS and F_w, the sensitivity of M_o to changes in $d\delta_{max}/dt$ varies as a natural log with respect to deposition rate. M_o is most sensitive at deposition rates <30 m Myr^{-1} (~2.3 mM increase for 10 m Myr^{-1} rate decrease), moderately sensitive at rates of 30–50 m Myr^{-1} (~0.9 mM per 10 m Myr^{-1} rate increase), and insensitive at rates >50 m Myr^{-1} (<0.4 mM per 10 m Myr^{-1} rate increase). Deposition rates are estimated to be 30–50 m Myr^{-1}, which is consistent with available, though imperfect, radiometric and chemostratigraphic constraints, as well as with average deposition rates calculated for Palaeozoic carbonate platforms[23]. Although instantaneous rates of deposition were probably higher, shallow marine carbonate accumulation is typically limited by accommodation space, and stratal thicknesses reflect average subsidence through the duration of sediment accumulation. For epicratonic and pericratonic environments typical of carbonate deposition, much of this time is represented by unconformities that coincide with parasequence and sequence-scale stratigraphic boundaries. Fortunately, lateral tracing of depositional boundaries and the continuity of our preserved isotopic trends suggests that, with rare exceptions, individual unconformities are short in duration compared to the total time represented by the sediment package. Our conservative estimates therefore ensure that our calculations reflect maximum possible values for M_o.

Received 24 October 2003; accepted 20 August 2004; doi:10.1038/nature02974.

1. Canfield, D. E., Habicht, K. S. & Thamdrup, B. The Archean sulfur cycle and the early history of atmospheric oxygen. *Science* **288,** 658–661 (2000).
2. Farquhar, J., Bao, H. & Thiemens, M. Atmospheric influences of the Earth's earliest sulfur cycle. *Science* **289,** 756–758 (2000).
3. Karhu, J. A. & Holland, H. D. Carbon isotopes and the rise in atmospheric oxygen. *Geology* **24,** 867–870 (1996).
4. Canfield, D. E. A new model for Proterozoic ocean chemistry. *Nature* **396,** 450–453 (1998).
5. Habicht, K. S., Gade, M., Thamdrup, B., Berg, P. & Canfield, D. E. Calibration of sulfate levels in the Archean ocean. *Science* **298,** 2372–2375 (2002).
6. Canfield, D. E. & Teske, A. Late Proterozoic rise in atmospheric oxygen concentration inferred from phylogenetic and sulphur-isotope studies. *Nature* **382,** 127–132 (1996).
7. Habicht, K. S. & Canfield, D. E. Isotope fractionation by sulfate-reducing natural populations and the isotopic composition of sulfide in marine sediments. *Geology* **29,** 555–558 (2001).
8. Anbar, A. D. & Knoll, A. H. Proterozoic ocean chemistry and evolution: a bioinorganic bridge? *Science* **297,** 1137–1142 (2002).
9. Kump, L. R. & Arthur, M. A. Interpreting carbon-isotope excursions; carbonates and organic matter. *Chem. Geol.* **161,** 181–198 (1999).
10. Staudt, W. J. & Schoonen, M. A. A. Sulfate incorporation into sedimentary carbonates. *Am. Chem. Soc. Symp.* **612,** 332–345 (1995).
11. Burdett, J. W., Arthur, M. A. & Richardson, M. A Neogene seawater sulfur isotope age curve from calcareous pelagic microfossils. *Earth Planet. Sci. Lett.* **94,** 189–198 (1989).
12. Lyons, T. W., Luepke, J. J., Schreiber, M. E. & Zeig, G. A. Sulfur geochemical constraints on Mesoproterozoic restricted marine deposition: Lower Belt Supergroup, northwestern United States. *Geochim. Cosmochim. Acta* **64,** 427–437 (2000).
13. Strauss, H. The isotopic composition of sedimentary sulfur through time. *Palaeogeogr. Palaeoclimatol. Palaeoecol.* **132,** 97–118 (1997).
14. Paytan, A., Kastner, M., Campbell, D. & Thiemans, M. H. Sulfur isotopic composition of Cenozoic seawater sulfate. *Science* **282,** 1459–1462 (1998).
15. Kampschulte, A., Bruckschen, P. & Strauss, H. The sulphur isotopic composition of trace sulphates in Carboniferous brachiopods: implications for coeval seawater, correlation with other geochemical cycles and isotope stratigraphy. *Chem. Geol.* **175,** 149–173 (2001).
16. Hurtgen, M. T., Arthur, M. A., Suits, N. & Kaufman, A. J. The sulfur isotopic composition of Neoproterozoic seawater sulfate: implications for a snowball Earth? *Earth Planet. Sci. Lett.* **203,** 413–429 (2002).
17. Luepke, J. J. & Lyons, T. W. Pre-Rodinian (Mesoproterozoic) supercontinental rifting along the western margin of Laurentia: geochemical evidence from the Belt-Purcess Supergroup. *Precambr. Res.* **111,** 79–90 (2001).
18. Whelan, J. F., Rye, R. O., deLorraine, W. & Ohmoto, H. Isotopic geochemistry of a mid-Proterozoic evaporite basin: Balmat, New York. *Am. J. Sci.* **290,** 396–424 (1990).
19. Gellatly, A. M. & Lyons, T. W. Trace sulfate in Mid-Proterozoic carbonates and the sulfur isotope record. *Geochim. Cosmochim. Acta* (in the press).
20. Azmy, K. *et al.* Dolomitization and isotope stratigraphy of the Vazante Formation, São Francisco Basin, Brazil. *Precambr. Res.* **112,** 303–329 (2001).
21. Kah, L. C., Lyons, T. W. & Chesley, J. T. Geochemistry of a 1.2 Ga carbonate-evaporite succession, northern Baffin and Bylot Islands: implications for Mesoproterozoic marine evolution. *Precambr. Res.* **111,** 203–234 (2001).
22. Frank, T. D., Kah, L. C. & Lyons, T. W. Changes in organic matter production and accumulation as a mechanism for isotopic evolution in the Mesoproterozoic ocean. *Geol. Mag.* **140,** 373–396 (2003).
23. Bosscher, H. & Schlager, W. Accumulation rates of carbonate platforms. *J. Geol.* **101,** 345–355 (1993).

24. Shen, Y., Knoll, A. H. & Walter, M. R. Evidence for low sulphate and anoxia in a mid-Proterozoic marine basin. *Nature* **423,** 632–635 (2003).
25. Shen, Y., Canfield, D. E. & Knoll, A. H. Middle Proterozoic ocean chemistry: Evidence from the McArthur Basin, northern Australia. *Am. J. Sci.* **302,** 81–109 (2002).
26. Brennan, S. T., Lowenstein, T. K. & Horita, J. Seawater chemistry and the advent of biocalcification. *Geology* **32,** 473–476 (2004).
27. Knoll, A. H., Hayes, J. M., Kaufman, A. J., Swett, K. & Lambert, I. B. Secular variation in carbon isotope ratios from Upper Proterozoic successions of Svalbard and East Greenland. *Nature* **321,** 832–838 (1986).
28. Grotzinger, J. P. Facies and evolution of Precambrian depositional systems: emergence of the modern platform archetype. *SEPM Spec. Publ.* **44,** 79–106 (1989).
29. Berner, R. A. Modeling atmospheric O_2 over Phanerozoic time. *Geochim. Cosmochim. Acta* **65,** 685–694 (2001).
30. Schlesinger, W. H. *Biogeochemistry* (Academic, San Diego, 1997).

Supplementary Information accompanies the paper on **www.nature.com/nature**.

Acknowledgements This work was supported by the NSF, the National Geographic Society, the Polar Continental Shelf Project (Natural Resources, Canada), and the University of Missouri Research Board.

Competing interests statement The authors declare that they have no competing financial interests.

Correspondence and requests for materials should be addressed to L.C.K. (lckah@utk.edu).

A new troodontid dinosaur from China with avian-like sleeping posture

Xing Xu[1,2] **& Mark A. Norell**[2]

[1]*Institute of Vertebrate Paleontology & Paleoanthropology, Chinese Academy of Sciences, PO Box 643, Beijing 100044, China*
[2]*American Museum of Natural History, Central Park West at 79th Street, New York City, New York 10024, USA*

Discovering evidence of behaviour in fossilized vertebrates is rare. Even rarer is evidence of behaviour in non-avialan dinosaurs that directly relates to stereotypical behaviour seen in extant birds (avians) and not previously predicted in non-avialan dinosaurs[1,2]. Here we report the discovery of a new troodontid taxon from the Early Cretaceous Yixian Formation of western Liaoning, China. Numerous other three-dimensionally preserved vertebrate fossils have been recovered recently at this locality, including some specimens preserving behavioural information[3]. The new troodontid preserves several features that have been implicated in avialan origins. Notably, the specimen is preserved in the stereotypical sleeping or resting posture found in extant Aves[4]. Evidence of this behaviour outside of the crown group Aves further demonstrates that many bird features occurred early in dinosaurian evolution[5,6].

Theropoda Marsh, 1881
Maniraptora Gauthier, 1986
Troodontidae Gilmore, 1924
Mei long gen. et sp. nov.

Etymology. *Mei* from Chinese, meaning to sleep soundly; *long* from Chinese, meaning dragon.

Holotype. IVPP (Institute of Vertebrate Paleontology and Paleoanthropology, Beijing) V12733, a nearly complete, fully articulated skeleton (Fig. 1).

Locality and horizon. Lujiatun, Shangyuan, Beipiao City, western Liaoning, China; lowest more fluvial, volcaniclastic beds of Yixian Formation, older than 128 and younger than 139 million years[7].

Diagnosis. *Mei long* is distinguishable from all other troodontids on the basis of extremely large nares extending posteriorly over one-half of the maxillary tooth row; closely packed middle maxillary teeth; maxillary tooth row extending posteriorly to the level of the preorbital bar; a robust, sub-'U'-shaped furcula; presence of a lateral process on distal tarsal IV; and the most proximal end of the pubic shaft is significantly compressed anteroposteriorly, and extends laterally just ventral to the articulation with the ilium.

Mei long is about 53 cm in length, similar in size to the basal dromaeosaurid *Microraptor zhaoianus* and the basal avialan *Archaeopteryx lithographica*[5,8,9]. IVPP V12733 is not an adult, as several cranial sutures are unfused, and although fused, sutures between the neural arches and centra are still apparent on the dorsal vertebrae. However, the holotype is also not a hatchling as caudal and sacral vertebral sutures are not apparent, the parietal is formed from a single element and there is complete fusion of astragalus and calcaneum, indicating that the individual is approaching maturity.

As in *Sinovenator changii* and basal dromaeosaurs[5], the skull is proportionally small (about 69% of the femoral length), the trunk short and the hindlimbs very long. Long hindlimbs relative to the trunk is a feature correlated with a knee-based avian running mechanism[10]; it is also present in the basal troodontids *Sinovenator* and *Sinornithoides*[11,12], the basal dromaeosaurid *Microraptor*, and the basal oviraptorosaurian *Caudipteryx*[5,10]. As in other troodontids[13,14] the numerous maxillary teeth (approximately 24) are tightly packed anteriorly (Fig. 2a, b). Unlike other troodontids, even the middle teeth lack inter-crown space. Posteriorly, the teeth are more stout and re-curved. As with other troodontids[5], the internarial bar is strap-like and 'T'-shaped. Additionally, a pneumatopore lies on the posterior quadrate surface; a prominent convexity lies lateral to the foramen magnum on the exoccipital/opisthotic; and the distally expanded pendulous paroccipital processes are vertical and apneumatic. The dentary nutrient foramina lie in a horizontal groove on the labial surface of the dentary as in other troodontids[13,15].

As in *Sinovenator changii* the dorsal vertebrae have fan-shaped neural spines and slender transverse processes, but lack pneumatic foramina[6]. The distal caudals are elongate, with a reduced centrum and a sulcus on their dorsal surface as in other troodontids[12]. The ilium is short and tapers posteriorly. The pubis is long and proximally thick, but is not mediolaterally compressed as in other troodontids including *Sinovenator changii*. The ischium is fairly short with a distally positioned obturator process and two small processes on the dorsal edge. The tibia has an anteroposteriorly wide proximal end, and a distal end with a thick lateral margin. As in basal dromaeosaurids and *Sinovenator*[16,17] the feet are subarctometatarsalian, and metatarsal III is reduced but still visible on the plantar surface (Fig. 1b). Metatarsal II bears a prominent medial flange and metatarsal IV a lateral one on the ventral surface, producing a longitudinal metatarsal palmar excavation. As in other deinonychosaurs, the second pedal digit is specialized with a hypertrophied claw, but is not developed to the same degree as seen in derived dromaeosaurids[5,18].

Mei long differs with respect to a number of features compared with most other troodontids. Many of these differences are similar to conditions seen in avialans and dromaeosaurids[5,17–19]. Laterally, the skull has an antorbital fossa that is much smaller than that of other non-avialan theropods (except for oviraptorosaurians[5]) and a large orbit that is apparently confluent with the infra-temporal fenestra (Fig. 2a, b). No postorbital is preserved, but if present it was undoubtedly small, as in *Archaeopteryx*[9]. As in avialans[19] and mononykines[20], there is no corresponding ascending postorbital process of the thin jugal to form a complete postorbital bar; however, there is a small dorsal expansion of the jugal at its posterior end (as in *Archaeopteryx*[19]), near where it contacts the quadrate, which is buttressed by an extremely small quadratojugal (Fig. 2a, b). The squamosal is also reduced and does not contact the quadrato-

Supplementary Information – Methods

Evidence for Low Marine Sulphate and the Protracted Oxygenation of the Proterozoic Biosphere (Kah, Lyons, and Frank)

CAS Preparation Methods:

CAS extraction followed methods modified from Burdett et al. (1989), Kampschulte et al. (2001), and Hurtgen et al. (2002). Approximately 100 g to 300 g whole-rock sample were trimmed to remove visibly weathered surfaces, crushed and hand-picked to remove chips containing weathered durfaced or secondary carbonate phases; samples were etched with 10% HCl to remove any remaining surficial contaminants. Rinsed and dried chips were powdered and subjected to a series of rinses. Samples from the Dismal Lakes Group underwent a 24 hour rinse with 5.25% NaOCl solution, followed by a 24 hour rinse with ultrapure Milli-Q water. A sodium hypochlorite rinse will effectively remove organic matter and organically bound sulfate, and is therefore critical when processing biogenically produced carbonate samples (Burdett et al., 1989). Labile, sulfate-containing polysaccharides, however, are not likely to survive early organic matter diagenesis and this step will have minimal affect on preserved kerogens in Precambrian samples. In the case of Precambrian samples, this rinse also serves to remove metastable sulfide minerals that might be oxidized during the extraction process. A secondary, 24 hour rinse with ultrapure Milli-Q water assured removal of any soluble sulfates within the sample. In the case of samples from the Society Cliffs Formation, which occur in close association with bedded gypsum and frequently contain evidence for disseminated gypsum, two additional 24 hour, ultrapure Milli-Q water rinses were performed to assure removal of associated soluble sulfates.

Powdered samples were then thoroughly rinsed in ultrapure Milli-Q water, filtered, and dried. Dried samples were dissolved slowly in 3N HCl. Once reaction ceased, samples were filtered to remove insoluble residues (primarily a small amount of particulate clay minerals), and an excess (100-200 mL) of a saturated $BaCl_2$ solution was added to the solute to precipitate $BaSO_4$. Rinsed, filtered, and dried $BaSO_4$ precipitates were then combined with an excess of V_2O_5 and analyzed for S-isotope composition at Indiana University on a Finnigan MAT 252 gas source mass spectrometer fitted with a peripheral elemental analyzer (EA) for on-line sample combustion. Sulfur isotope compositions are expressed in standard delta-notation as permil (‰) deviations from VCDT, with analytical error of <0.01‰, calculated from replicate analyses of laboratory standards.

Supplementary Information – Data

Evidence for Low Marine Sulphate and the Protracted Oxygenation of the Proterozoic Biosphere (Kah, Lyons, and Frank)

Supplementary Data Table 1. CAS data from Society Cliffs Formation and Dismal Lakes Group[1].

Sample	Height (meters)	$\delta^{34}S$ (‰ VPDB)	$[SO_4^{2-}]$ (ppm)
BY97-175-1	17.5	25.3	196
BY97-175-2	17.5	25.2	196
BY97-270	27.0	23.6	3000*
BY97-365	36.5	27.0	196
BY97-441	44.1	22.6	6111*
BY97-558-1	55.8	25.2	1092*
BY97-558-2	55.8	25.3	1092*
BY97-1263-1	126.3	28.6	261
BY97-1263-2	126.3	28.4	261
BY97-1317	131.7	28.4	156
BY97-1337	133.7	25.1	164
BY97-1352-1	135.2	26.1	1147*
BY97-1352-2	135.2	26.1	1147*
BY97-1565	156.5	31.2	176
BY97-1840-1	184.0	32.6	181
BY97-1840-2	184.0	32.7	181
BY97-1986	198.6	33.7	35
BY97-2045	204.5	32.8	170
BY97-2190-1	219.0	36.7	138
BY97-2190-2	219.0	37.8	138
BY97-2556	255.6	33.2	127
BY97-2774	277.4	30.6	106
BY97-2902-1	290.2	31.2	136
BY97-2902-2	290.2	31.3	136
BY97-2916	291.6	32.5	448*
BY97-3044-1	304.4	34.3	130
BY97-3044-2	304.4	37.5	130
BY97-4191-1	419.1	29.1	111
BY97-4191-2	419.1	38.5	111
BY97-4406-1	440.6	31.7	211
BY97-4406-2	440.6	39.8	211
BY97-4406-3	440.6	35.7	211
BY97-4989	498.9	29.2	300
BY97-5210	521.0	30.5	163
BY97-5694-1	569.4	23.6	234
BY97-5964-2	569.4	24.0	234
BY97-6022-1	602.2	27.9	142
BY97-6022-2	602.2	28.5	142
BY97-6741	674.1	26.6	97
BY97-7031-1	703.1	27.2	64
BY97-7031-2	703.1	26.9	64
BY97-8261	826.1	20.1	50
BY97-8625-1	862.5	25.7	56
BY97-8625-2	862.5	25.6	56

DL1-28.8-1	28.8	30.6	76
DL1-28.8-2	28.8	30.9	76
DL1-42.3-1	42.3	28.4	35
DL1-42.3-2	42.3	28.8	35
DL1-42.3-3	42.3	29.2	35
S2-46-1	59.0	30.7	45
S2-46-2	59.0	31.1	45
S2-53-1	66.0	22.5	47
S2-53-2	66.0	20.1	47
DL1-88-1	88.0	29.0	7
DL2-118	118.0	26.4	5
DL2-118-1	118.0	25.7	5
DL1-168	168.0	19.3	16
DL1-168-1	168.0	19.4	16
DL1-201	201.0	17.3	14
DL1-220	220.0	21.6	11
DL2-253	253.0	33.2	42
DL1-263	263.0	23.0	15
DL1-318	318.0	23.1	13
DL2-345	345.0	26.5	17
DL1-39.9T	469.9	17.5	36
DL1-46T	503.0	21.2	6

1. Carbonate-associated sulfate (CAS) from the 1.2 Ga Society Cliffs Formation (BY- samples) and the 1.3 Ga Dismal Lakes Group (DL1-, DL2-, and S2- samples). All samples were collected from continuous measured sections. Sulfate concentrations marked by asterisks are anomalously high and suggest that initial sample preparation did not succeed in removing disseminated gypsum. Replicate samples typically vary in S-isotope composition by <<1‰; a few anomalous replicate readings (samples BY97-3044, BY97-4191, and BY97-4406) likely represent contamination of the sample during loading and analysis on the mass spectrometer.

Supplementary Data Table 2. CAS data from McNamara Group and Belt Supergroup[1].

Sample	Height (meters)	$\delta^{34}S$ (‰ VPDB)	$[SO_4^{2-}]$ (ppm)
PC 360.8	360.8	29.0	*
PC 368.3	368.3	26.4	9.6
PC 373.5	373.5	32.1	17.4
PC 379.5	379.5	31.5	25.2
PC 384.8	384.8	16.5	21.9
PC 388.5	388.5	31.3	16.8
PC 399.0	399.0	27.8	51.5
PC 405.8	405.8	33.0	92.3
PC 420.0	420.0	30.3	1.8
PC 424.5	424.5	27.4	39.9
PC 430.5	430.5	25.0	92.0
PC 440.6	440.6	35.1	1.8
PC 450.0	450.0	37.2	87.5

PC 462.0	462.0	35.2	91.1
PC 465.0	465.0	37.2	86.0
PC 472.5	472.5	30.6	11.1
PC 486.0	486.0	36.4	62.0
PC 502.5	502.5	27.9	*
PC 507.0	507.0	30.4	73.7
PC 528.0	528.0	30.1	*
PC 543.0	543.0	37.3	62.0
PC 545.3	545.3	14.1	73.7
PC 546.0	546.0	37.0	-
HF 4.6	4.6	11.1	2.5
HF 6.1	6.1	12.0	19.2
HF 10.7	10.7	-	3.2
HF 14.6	14.6	-	9.0
HF 22.9	22.9	6.9	10.3
HF 24.4	24.4	10.9	9.6
HF 42.7	42.7	-	16.3
HF 47.2	47.2	11.9	8.2
HF 51.8	51.8	12.7	*
HF 54.9	54.9	-	18.3
HF 59.4	59.4	14.0	10.8
HF 73.2	73.2	-	22.8
HF 79.9	79.9	-	20.0
HF 85.3	85.3	14.0	3.2
HF 92.4	92.4	-	1.0
HF 115.8	115.8	13.0	*
HF 121.9	121.9	-	1.1
HF 140.2	140.2	17.8	46.1
HF 152.4	152.4	-	8.6
HF 182.9	182.9	-	10.8
HF 189.0	189.0	20.3	92.5
HF 195.1	195.1	18.5	66.8
HF 216.4	216.4	13.0	16.7
HF 222.5	222.5	13.1	24.6
HF 228.6	228.6	13.3	82.4
HF 234.7	234.7	-	21.7
HF 240.8	240.8	-	9.2
HF 246.9	246.9	-	9.6
HF 277.4	227.4	12.0	10.2
HF 307.8	307.8	9.8	9.0
HF 317.0	317.0	9.0	46.8
HF 335.3	335.3	12.6	21.9
HF 353.6	353.6	7.6	56.4
HF 368.8	368.8	3.6	35.4
HF 381.0	381.0	-1.1	94.3
HF 387.1	387.1	15.1	54.4
HF 339.3	399.3	15.1	*
HF 411.5	411.5	14.9	27.1
HF 431.3	431.3	4.7	84.8
HF 438.9	438.9	16.6	-
HF 445.0	445.0	15.6	115.6

1. Carbonate-associated sulfate (CAS) from the 1.7 Ga McNamara Group, Australia (PC-samples) and the 1.45 Ga Helena Formation, Belt Supergroup, Montana (HF- samples). All samples were collected from continuous measured sections. Asterisks denote sulphate concentrations below detection; dash denotes no value available. Data included here, with

permission, from Gellatly (2002) [Trace sulfate in Mesoproterozoic carbonates: Implications for ocean-atmospheri oxygen availability: unpublished M.S. thesis, University of Missouri-Columbia, 48 p.] and Gellatly and Lyons [Trace sulfate in Mesoproterozoic carbonates: Geochimica et Cosmochimica Acta (*accepted*)].

Supplementary Information – Figures

Evidence for Low Marine Sulphate and the Protracted Oxygenation of the Proterozoic Biosphere (Kah, Lyons, and Frank)

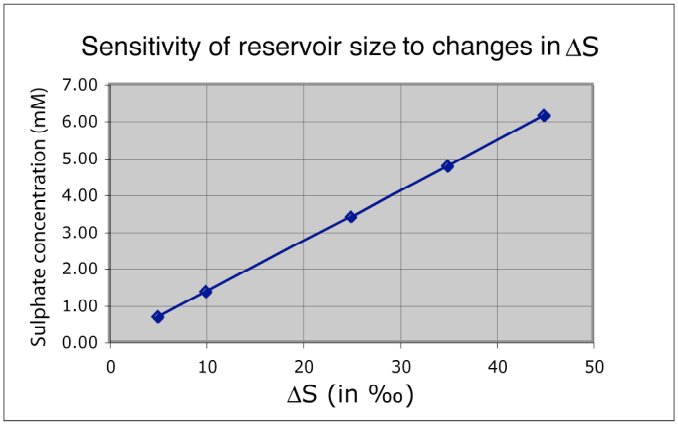

Supplementary Figure 1. Sensitivity of sulphate reservoir size to changes in DS. M_o is most sensitive to changes in ΔS, wherein a 10% change in ΔS (~5‰) results in a 0.7 mM change in M_o. In our calculations, we have allowed the average maximum fractionation during BSR (ΔS) to vary with time as indicated by empirical data recorded in Proterozoic strata (compiled by Canfield and Teske, 1996).

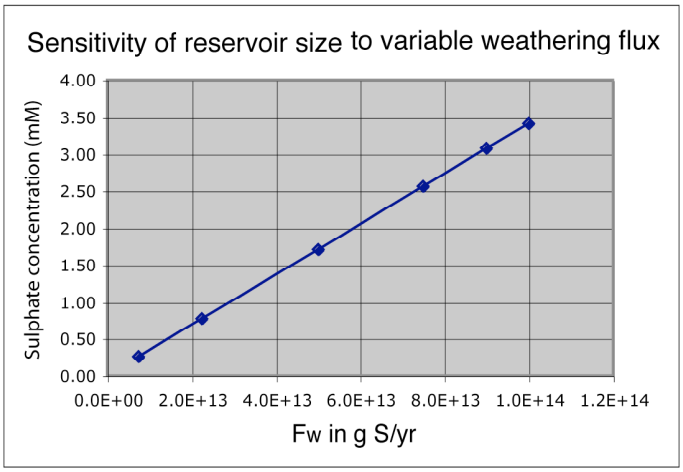

Supplementary Figure 2. Sensitivity of sulphate reservoir size to changes in weathering flux. In our model, a 10% decrease in F_w results in a 0.3 mM reduction in M_o. Because of uncertainties regarding the magnitude of Proterozoic weathering, we have used modern weathering fluxes to ensure that our calculations reflect *maximum* values for M_o.

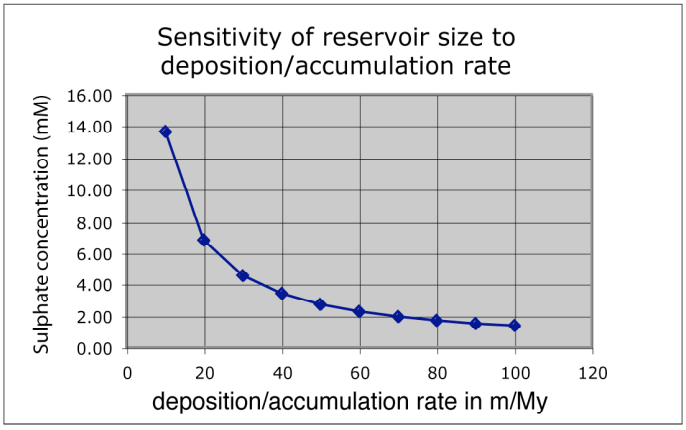

Supplementary Figure 3. Sensitivity of sulphate reservoir size to changes in deposition/accumulation rate. the sensitivity of M_o to changes in $d\delta_{max}/dt$ varies as a natural log with respect to deposition rate. M_o is most sensitive at deposition rates <30 m/My (~2.3 mM increase for 10 m/My rate decrease), moderately sensitive at rates of 30-50 m/My (~0.9 mM per 10 m/My rate increase), and insensitive at rates >50 m/My (<0.4 mM per 10 m/My rate increase). Our conservative estimates of 30-50 m/My ensure that our calculations reflect *maximum* possible values for M_o.